New Journal of Physics
The open-access journal for physics

Pump and probe ultrafast electron dynamics in LiH: a computational study

M Nest[1], F Remacle[2,3] and R D Levine[3,4,5]

[1] Institut für Chemie, Universität Potsdam, 14476 Potsdam, Germany
[2] Département de Chimie, B6c, Université de Liège, B4000 Liège, Belgium
[3] The Fritz Haber Research Center for Molecular Dynamics, The Hebrew University of Jerusalem, Jerusalem 91904, Israel
[4] Department of Chemistry and Biochemistry, The University of California Los Angeles, Los Angeles, CA 90095-1569, USA
E-mail: rafi@chem.ucla.edu

New Journal of Physics **10** (2008) 025019 (24pp)
Received 28 September 2007
Published 29 February 2008
Online at http://www.njp.org/
doi:10.1088/1367-2630/10/2/025019

Abstract. A time-dependent multiconfiguration method with a large electronic basis set is used to compute the response of all the electrons of LiH to a few-cycle intense pump field followed by a probe pulse. The ultrashort pump pulse excites a coherent superposition of stationary electronic states and, by changing the pump parameters such as intensity, duration, polarization and phase of carrier frequency, one can steer the motion of the electrons. Particular attention is given to the control provided by the polarization and by the phase. For example, a change in polarization is used to select an electronic wave packet that is rotating in a plane perpendicular to the bond or rotation in a plane containing the bond. The electronic wave packet can be probed by a delayed second pulse. This delayed probe pulse is also included in the Hamiltonian with the result that the frequency dispersed probe spectrum can be computed and displayed as a two-dimensional plot.

[5] Author to whom any correspondence should be addressed.

Contents

1. Introduction

With a total of four electrons, LiH early on became 'the workbench of theoretical chemistry' [1]. Already in 1977, Mulliken and Ermler [2] said that 'numerous *ab initio* calculations have been made on LiH'. Some of the then more recent ones that they cite include Boys and Handy [3], Bender and Davidson [4], Docken and Hinze [5], Meyer and Rosmus [6], the valence bond of Yardley and Balint-Kurti [7] and the early time-dependent Hartree–Fock calculations by Stewart *et al* [8]. More recent work including spectroscopic studies has been reviewed by Stwalley and Zemke [1] and Gadea [9]. The application of a time-dependent point of view to compute the stationary states of LiH is discussed in our recent papers [10, 11] with related references therein.

Mulliken [12] early on pointed out that the motion of the nuclei results in extensive reorganization of the electronic charge distribution of LiH. Here, however, we discuss a post-Born–Oppenheimer regime where the motion of the electrons is pumped and probed on a timescale short compared to the vibration of the nuclei (24 fs in the ground state (GS) of LiH). Such purely electron dynamics is made possible because an ultrashort UV pulse can create a non-stationary electronic state and therefore the electronic reorganization does not require the nuclei to move. The electron dynamics as computed here is therefore different from what occurs upon the failure of the Born–Oppenheimer approximation [13]–[18], a failure induced by the motion of the nuclei. The additional reason [19] for looking at such a ultrafast process is that by controlling the coherent motion on several electronic states, one may be able to control the motion of the nuclei and thereby manipulate the chemical outcome.

One can think of the state that is optically accessed at ultrashort times as a coherent linear combination of stationary electronic states. The time evolution is then described as due to the interference between different states. The amplitudes of the different states in the wave packet are determined by the parameters of the pulse and it is thereby possible to control the dynamics of the electrons. To probe the coherent dynamics [20], we apply a second pulse delayed with respect to the pump. The probe pulse needs also to be ultrashort in order that it monitors the coherent dynamics prior to the dephasing induced by the onset of the motion of the nuclei.

Our theoretical work is motivated by the spectacular progress in attosecond physics [21]–[38] where few-cycle pulses in the soft x-ray region have been used to control ionization in atoms and simple molecules [20], [39]–[43]. The shorter wavelength of such

pulses means that a few cycles of light can be contained in an envelope whose width is sub-femtoseconds, thereby giving rise to new physics. The chemical properties of molecules are governed by the valence electrons. To excite bound motions of the valence electrons requires light of lower frequencies, in the range of up to, say, 15 eV. The envelope of the pulse must then necessarily be longer [44], from about one to a few femtoseconds. It is currently not yet possible to experimentally generate few-cycle ultrashort laser pulses in the energy range of interest for electronic spectroscopy, but progress is being made [44, 45].

We explore here the interaction of a molecule with such intense few-cycle UV pulses at a realistic quantitative level of computation. It is shown that even at the high powers required to pump a sizeable fraction of molecules it is possible to maintain tight control over the dynamics of the electrons. Other recent studies of ultrafast processes include the work on localization of electrons by the laser pulse [46]–[48], on LiCN [49], on inducing ring currents [50, 51], on the importance of correlation effects in charge migration [52]–[54] and on other intense field effects on molecules [55]–[66]. We pay special attention to the control of the electron dynamics that is allowed by the physical parameters of the pump and to the probing of the resulting coherent motion.

2. Time-dependent multiconfiguration method

The dynamics is unfolding in time using a multideterminant approach [10, 11] where the N electron wavefunction $\Psi(\mathbf{x}_1, \ldots, \mathbf{x}_N; t)$ is expressed as a linear combination of Slater determinants with time-dependent coefficients and where the determinants themselves are made from n *time-dependent* (spin) orbitals $\varphi_j(\mathbf{x}; t)$. As will be discussed shortly, these orbitals are chosen to adapt to the temporal changes in the electronic structure

$$\Psi(\mathbf{x}_1, \ldots, \mathbf{x}_N; t) = \sum_J A_J(t) \det \left| \varphi_{j_1}(\mathbf{x}_1; t) \cdots \varphi_{j_N}(\mathbf{x}_N; t) \right|, \tag{1}$$

J is an N-tuple index that enumerates the N spin orbitals that appear in the determinant and a shorthand notation for the determinant is $|J(t)\rangle$. Because of the antisymmetry, there are only $n!/N!(n-N)!$ determinants. $\mathbf{x}_i$ specifies the space and spin coordinates of electron i and the $n/2$ spatial orbitals are expressed as a linear combination of M atomic basis functions. As emphasized below, the orbitals $\varphi_j(\mathbf{x}; t)$ are allowed to adjust with time. Therefore we need only $n/2 = 5 < M$ spatial orbitals to achieve high accuracy, where M is the size of the atomic basis set. We do not freeze the core electrons so that for LiH, $N = 4$. The atomic basis set is the triple zeta Gaussian basis set with polarization and diffuse functions, 6-311++G(2df,2p) [67–70], which comprises $M = 49$ Cartesian atomic orbitals. We compute the electronic dynamics for excited singlet states. For the 4 electrons/5 orbitals system under consideration, there are 210 singlet determinants and *all* are included in the basis set, meaning that all are included in equation (1). We emphasize that because the 5 molecular orbitals (MO) used to generate the 210 configurations are reoptimized at each time step, the basis of determinants that we use actually corresponds to a much larger number of configurations than if a fixed basis of MOs is used. This is analogous to the multi-configuration self-consistent field (MC-SCF) approach to time-independent electronic structure theory. As discussed below, we verify, by comparing to well-established quantum chemistry procedures, that all valence excited singlet states of LiH are accessed by an intense pump pulse acting on the GS. It takes an intense pulse because, of course, some of the excited states can only be reached by multiphoton transitions.

To determine the post-Born–Oppenheimer dynamics, namely for such short times that the atomic nuclei do not yet move, it is sufficient to take the Hamiltonian of the system for frozen nuclear positions. In addition, we assume that the molecular axis is aligned with the z-axis of the laser field, which is reasonable for the strong fields considered here [71]. The Hamiltonian consists of the conventional N electron Hamiltonian, including, as usual, the nuclear Coulomb repulsion terms plus any time-dependent external field that can perturb the electrons. We couple the molecule to the electric field $\mathbf{E}(t)$ of the pump pulse in the dipole approximation, resulting in a sum of one electron operators,

$$V = \left(\sum_{i=1}^{N} \mathbf{r}_i\right) \mathbf{E}\,(t)\,. \tag{2}$$

The field envelope is Gaussian, centered at t_0 with a width σ and a carrier frequency ω_0. A few cycle pulse means that $\omega_0\sigma > 2\pi$ but not much larger. ϕ is the phase of the carrier wave with respect to the envelope. The vector $\mathbf{E}$ is the field strength whose components in the different directions define the polarization of the pulse

$$\mathbf{E}(t) = \mathbf{E}(\exp(-(t-t_0)^2/2\,\sigma^2))\cos(\omega_0 t + \phi). \tag{3}$$

When a pump is followed by a probe pulse, then it too has the same functional form for the electric field $\mathbf{E}\,(t)$, except that it is delayed with respect to the pump, meaning that its envelope is centered at $t_0 + \Delta t$, where Δt is the time delay. Also, the width in time of the envelope and the frequency and phase of the carrier wave can be different. As is intuitively reasonable, we find that it is advantageous to have the pump pulse as short as necessary for creating a non-stationary electronic state. That it will then be rather broad in frequency does not appear to be a disadvantage. Also, the pump field strength $|\mathbf{E}|$ is chosen high so as to drive as many molecules as possible to states above the threshold for ionization.

To propagate the wavefunction, we use equations of motion derived from a variational principle [10, 11]. This Dirac–Frenkel variational principle has been very extensively used [72] to derive the equations of motion for distinguishable particles, e.g. nuclei. A recent example is the work of Meyer and co-workers [73]–[75]. The time evolution of the amplitudes $A_J(t)$ of the different determinants that make up the wavefunction is generated by the full Hamiltonian

$$\mathrm{d}A_J(t)/\mathrm{d}t = -(\mathrm{i}/\hbar)\sum_K \langle J(t)|\,H\,|K(t)\rangle A_K(t). \tag{4}$$

Then the time dependence of the orbitals can be restricted to be due only to the need to change the space spanned by the $n/2$ spatial functions and this is possible when $(n/2) < M$, where M is the size of the atomic basis set [10, 11]. The equations of motion are solved by representing operators as matrices in the M-dimensional atomic basis set. The initial state for the time propagation is taken to be the GS so that any subsequent time dependence is due to the switching on of the pump field. To monitor the dynamics, the pump pulse is followed by a probe pulse.

The time dependence of the spatial orbitals and of the expansion coefficients $A_J(t)$ does not necessarily cease when the field is switched off. This is because a very short pulse sets up a coherent superposition of eigenstates and so the electronic charge density will continue to move with time as is discussed below. The orbitals dynamically adjust to this changing density. Even so, one can define stationary states and the time-dependent wavefunction can be expanded as a coherent combination of these states. In other words, the stationary states and eigenstates of the electronic Hamiltonian are not single configurations but are superpositions of determinants.

Table 1. Energetics and dipole strengths, all in (au), of excited states of LiH.

Excited state	$E_{\rm exc}$ (au)	Dipole μZ (au)	Transition dipole $\langle\Psi\|\mu_{x,y}\|{\rm GS}\rangle$	Transition dipole $\langle\Psi\|\mu_z\|{\rm GS}\rangle$	$E_{\rm n}$ Figure 1(a)	$E_{\rm n}$ Figure 1(b)
$^1\Sigma^+$	0.1139	−2.031		1.157	0.118	0.114
$^1\Pi$	0.1502	−0.193	1.521		0.152	0.149
$^1\Sigma^+$	0.1961	3.259		−0.421	0.200	0.196
$^1\Sigma^+$	0.2095	−5.150		0.038	0.214	0.210
$^1\Pi$	0.2167	−0.186	0.225		0.222	0.217
$^1\Sigma$	0.2300	2.556		−0.551	0.235	0.230
$^1\Sigma$	0.2650	5.375		−0.873	0.272	0.263
$^1\Pi$	0.2721	−0.177	−0.069		0.272	0.267
$^1\Delta$	0.3558	−0.182				0.355–0.360

This is also what is found [10, 44] when quantum chemistry procedures that allow for configuration interaction compute the excited states of LiH.

3. Pumping the excited states of LiH

Table 1 shows the energies and transition dipoles of the excited states of LiH computed using the well-established MOLPRO electronic structure package [76]. The MOLPRO computation is at the MC-SCF (multi) level for four active electrons using the same basis set as for the dynamics. Including the GS, ten states are computed simultaneously: six $^1\Sigma^+$, three $^1\Pi$ and one $^1\Delta$ states. The $^1\Delta$ state is above the vertical ionization threshold of LiH (about 0.29 au [77]) and it is used below as the state that the probe pulse pumps to.

The preliminary step is to compute a time-dependent electronic wavefunction with the pump pulse as part of the Hamiltonian and with the GS as the initial state at time zero. Then we can extract the excited states energies and amplitudes and validate the procedure by comparing with the results shown in table 1.

To compute the spectrum, the wavefunction $\Psi(t)$, equation (1), is propagated up to a time t when the pump pulse is effectively over and then for an additional time τ during which interval the molecule is unperturbed. The autocorrelation function [78] $\langle\Psi(t)|\Psi(t+\tau)\rangle$ is computed and its Fourier transform with respect to τ is performed. The longer the time interval τ, the better will be the resolution of the Fourier transform, that defines the excitation spectrum. In terms of the, initially unknown, orthonormal eigenstates of the electronic Hamiltonian, the autocorrelation function is diagonal. Upon Fourier transform, it will result in a series of peaks. The width of the peaks is not inherent but determined by the range of the time interval τ. For LiH, the location of the peaks is reported in table 1 and their heights are shown in the excitation spectra that are the subject of figure 1. The autocorrelation function is computed numerically as a bilinear sum

$$\langle\Psi(t)|\Psi(t+\tau)\rangle = \sum_{J,K} A_J^*(t) A_K(t+\tau)\langle J(t)|K(t+\tau)\rangle. \tag{5}$$

The cross correlation of the determinantal wavefunctions is computed from the time evolution of the orbitals $\varphi_j(\mathbf{x};t)$, cf equation (1). The autocorrelation function can also be written as an expansion in eigenstates. From such an expansion, equation (6), it is clear that the Fourier

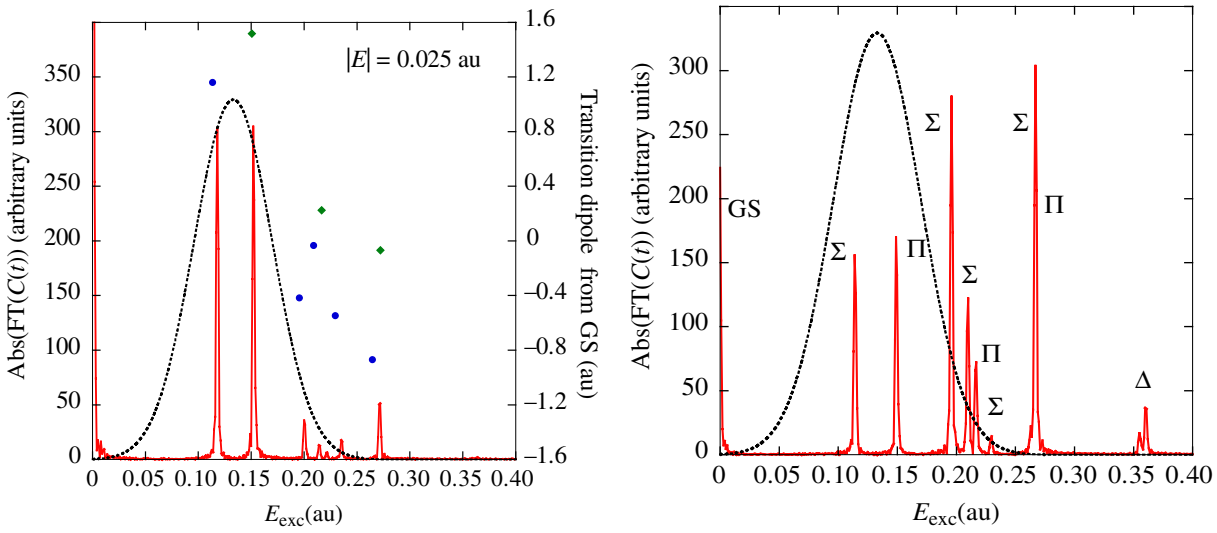

Figure 1. Excitation spectrum (full line, arbitrary units) obtained as the Fourier transform of the autocorrelation of the non-stationary electronic wavefunction at the end of the excitation pulse versus frequency. The excitation pulse (equation (3)) is polarized in the xy-direction and has a Gaussian envelope, and the phase shift ϕ is set to zero. The frequency components of the pulse are shown as a dashed line. (a) A moderate intensity, $|E| = 0.025$ au. To interpret the spectrum, shown are the transition dipole moments (solid circles for the z-component and solid diamonds for the x- and y-components, scale on the right ordinate) computed with the MOLPRO electronic structure package at the MC-SCF (multi) level for four active electrons. Note that the scale of the transition dipole moment is going from negative to positive and the location of the marker along the abscissa is at the energy computed by MOLPRO. (The energies of the excited states as well as their transition dipoles are given in table 1.) It is seen that at this intensity and carrier frequency, $\omega_0 = 0.133$ au, the primary states that are populated are the lowest excited Σ^+ and Π states that are both allowed by the one-photon selection rules and are well within the frequency span of the pulse. (b) At higher field strength ($|E| = 0.05$ au, peak intensity $= 8.75 \times 10^{13}\,\mathrm{W\,cm^{-2}}$), the next group of excited states (four of Σ^+ symmetry and two of Π) is accessed by two-photon transitions. Also seen in the spectrum is a metastable Δ state, whose energy is above the ionization potential (IP) of LiH (0.29 au) [77]. This state cannot be accessed from the GS by a one-photon transition because of selection rules, and it is essentially absent in (a). That is why we use the singlet Δ to probe the coherent superposition of the lowest excited Σ^+ and Π states created by the pump pulse, see figure 9.

transform of the autocorrelation function is the excitation spectrum. It shows frequency, the locations $\omega_n = E_n/\hbar$ and the intensity $|c_n|^2$ of the different transitions in figure 1,

$$\langle \Psi(t)\,|\Psi(t+\tau)\rangle = \sum_n |c_n|^2 \exp(-\mathrm{i}\,E_n\tau) \xrightarrow{\mathrm{FT}} \sum_n |c_n|^2 \delta\,(\omega-\omega_n)\,. \tag{6}$$

The delta function is broadened because the interval of propagation τ is finite.

Because the laser field is not introduced as a perturbation but is part of the Hamiltonian, electronic states n that are not allowed in the first order of perturbation theory, meaning that their dipole strength from the GS is zero, cf table 1, can still be seen in the spectrum. However, this only occurs when the pump intensity is high and this possibility of multiphoton transitions is emphasized by noticing the differences between the two panels of figure 1.

Figure 1(a) shows the excitation spectrum generated by a moderately intense pump pulse, ($|E| = 0.025$ au $\simeq 2.2 \times 10^{13}$ W cm^{-2}). The states accessed are primarily the excited states of LiH that can be pumped by dipole-allowed one-photon transitions from the GS. The pump pulse is short ($\sigma = 40/\sqrt{2}$ au ≈ 0.68 fs) and polarized at an angle of $\pi/4$ to the molecular axis (along the x–z-direction), so that both Σ^+ and Π states can be reached. The carrier frequency ($\omega_0 = 0.133$ au) is chosen to be about midway between the lowest excited Σ^+ and Π states so that they are about equally populated. The phase shift ϕ in equation (3) is set to 0. Higher-lying excited Σ^+ and Π states that do have, see table 1, oscillator strength from the GS are only weakly excited because their excitation frequency is barely contained within the frequency span of the pump pulse, also shown in the plot. At the same carrier frequency and pulse width but with a higher laser power ($|E| = 0.05$ au $\simeq 8.75 \times 10^{13}$ W cm^{-2}) (figure 1(b)), the higher states are reached by two photon transitions. At the higher intensity, the spectrum also shows such states as Δ that by dipole selection rules cannot be excited by one photon from the GS. At the carrier frequency of the pulse, $\omega_0 = 0.133$ au, the singlet Δ state whose excitation energy is 0.356 au, cf table 1, is most likely reached by a three-photon transition. Since in this computation the laser is polarized in the xz-plane, the $^1\Delta$ is most likely accessed by one x-polarized followed by two z-polarized photons or by other suitable combinations.

In section 4, we use a delayed probe pulse to excite to the Δ state as a diagnostic of which states are coherently accessed by the pump pulse. Of course, the energy range in question is above the ionization threshold so any such states will autoionize.

Equation (6) shows that the height of a peak in the Fourier transform with respect to τ of the autocorrelation function $\langle \Psi(t) | \Psi(t+\tau) \rangle$ of the wavefunction $|\Psi(t)\rangle$ at a time t after the pulse is the weight, $|c_n|^2$ of the nth eigenstate after the excitation is over. Figure 2 illustrates the so-called state-averaging effect, which is intrinsic for the multi-configuration time-dependent Hartree–Fock (MCTDHF) procedure. As mentioned above, the time-dependent orbitals adjust with time to the state that is to be represented. Initially the orbitals are optimized for the GS. At the higher intensities as shown in figure 1(b), there is significant depletion of the GS to a point where a population inversion is achieved. The orbitals then adjust to the excited state and the GS energy seems to rise. This correlation between the depletion of the GS and the quality of its description is shown in figure 2. This is an expanded scale of the spectrum shown in figure 1 in the vicinity of the GS peak.

Another view of the role of the pulse intensity is obtained by plotting the autocorrelation function of the GS as advocated by Heller [78] for ordinary electronic spectroscopy. In the present notation, this is the function $C_{\rm GS}(\tau) = \langle \Psi(0) | \Psi(\tau) \rangle$. Since we invariably start the system in the ground electronic state, another form of this autocorrelation function is $C_{\rm GS}(\tau) \equiv \langle {\rm GS} | \Psi(\tau) \rangle$. This definition allows one to think of $C_{\rm GS}(\tau)$ as the 'survival' probability of the GS [78, 79]. As shown in figure 3, at the higher intensity that is used to compute the results shown in figure 1(b) and when the laser is polarized along the molecular axis, about 60% of the GS is depleted. Also note in figure 3 that the GS is depleted most effectively when the laser field is at maximal amplitude. This correlation is at the heart of the coherent control of the outcome that we discuss below.

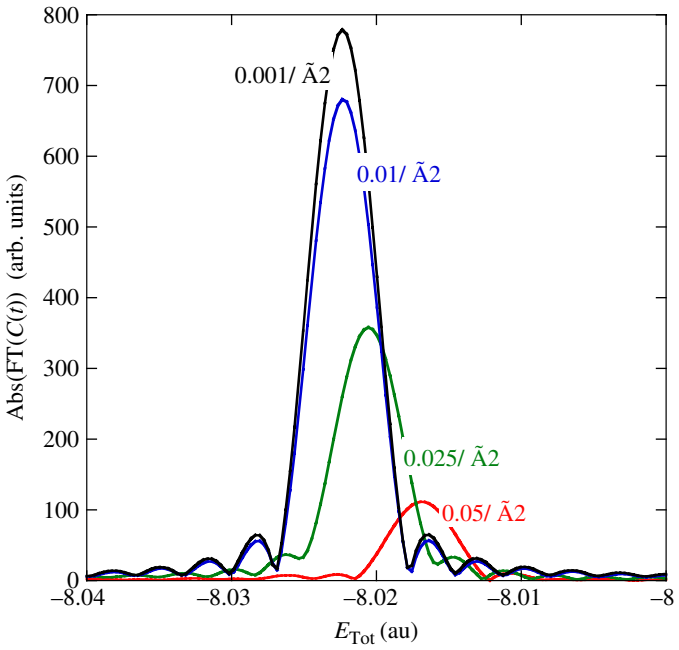

Figure 2. The spectrum obtained as the Fourier transform of the autocorrelation of the non-stationary electronic state at the end of the excitation pulse, same as figure 1, but on an expanded frequency scale in the close vicinity of the GS. Computed for the same pulse parameters as in figure 1 but for a series of different pulse intensities in the xz-direction, as indicated in the figure. The GS energy shifts because of the state averaging effect of the time-adapting orbitals. See text.

At the same intensity shown in figure 3 and if the laser is polarized along the zx-direction, already about 90% of the GS is depleted. Dipole selection rules determine which states can be excited. For polarization along the z-direction, the Σ^+ GS can be one photon pumped to the lowest excited Σ^+ and then higher Σ^+ states can be reached by multiphoton transitions. The allowed transitions for x-polarization are that the GS can be pumped to the lowest Π state and then multiphoton transitions can reach higher states, of both Σ^+ and Π symmetry. For polarization along the xz-direction, it is also possible to connect the GS coherently to the first excited Σ^+ state and to the higher-lying first excited Π state, what is not possible for a pure z-polarization. When the z-polarized field is reduced by a factor of 5 the depletion is only about 10% and one reaches the perturbative limit of low depletion, about 1%, when the field is further reduced by another factor of 5. Then, for a z-polarized field only the lowest excited Σ state is populated. As a check we verify that under the same intensity and duration, for an x-polarized field only the lowest excited Π state is accessed.

An important control parameter is the polarization of the laser pulse. We first discuss the role of laser polarization in the frequency domain, as shown in figure 4. The three panels in figure 4 show that up to and including intermediate intensities, 0.025 au, same as used in figures 1–3 and same carrier frequency, one-photon selection rules act as reliable propensity rules as to which states can be accessed. For a laser polarized perpendicular to the molecular axis, the main transition is to the lowest excited Π state with much weaker, two-photon

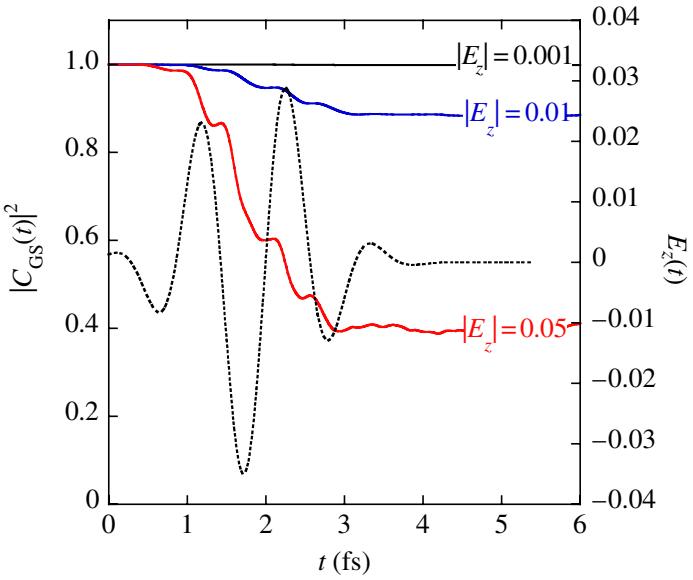

Figure 3. The autocorrelation function of the GS shown for a time range that corresponds to the excitation pulse and shortly thereafter. Note that what is computed here is different from equation (6). Shown is $C_{GS}(t) = \langle\Psi(t=0)|\Psi(t)\rangle$ for several intensities, where the initial state here and elsewhere is the GS, $|\Psi(t=0)\rangle = |GS\rangle$. The pulse is polarized in the z-direction and the value of the phase shift in equation (3) is set equal to 0. The time profile, right ordinate, is shown for the intensity of $|E| = 0.05$ au.

transitions via the Π state to higher excited Σ^+ states. For a laser polarized along the molecular bond, middle panel, the spectrum is complementary: the main transition is to the lowest excited Σ^+ state with much weaker, two-photon transitions via the Σ^+ state. The lower panel is for a polarization along the zx-direction at the same total intensity, meaning that the field in each direction is $1/\sqrt{2}$ of its value in the other two panels. The occupancy of the lowest excited Π state is indeed reduced by $1/2$.

To reliably compute the Rydberg and other high-lying states of LiH [9] one needs a much larger atomic basis set and this is prohibitive in the present stage of development of the time-adapting code that is needed to compute the dynamics.

The role of the polarization of the laser pulse in controlling the dynamics of the electrons is made vivid by examination of the charge distribution in the time domain. Before the pump, the distribution in the GS is cylindrically symmetric about the bond. When the origin of coordinates is placed at the center of mass, it is near the Li atom. The lighter H atom is further away from the origin. We expect that in the GS there is an excess of negative charge on the H atom, so that the center of (negative) charge is on the z-axis, off the center of mass and in a direction that we define to be negative. Upon using a pump polarized in the z-direction, we expect to excite a Σ^+ state where the charge is more evenly distributed on the two atoms. Unless the intensity is high, a significant amplitude remains on the GS. So the time-dependent wavefunction is a coherent superposition of the ground and first excited Σ^+ states, meaning that the center of the charge distribution (or, equivalently, the electronic dipole moment) remains along the z-axis,

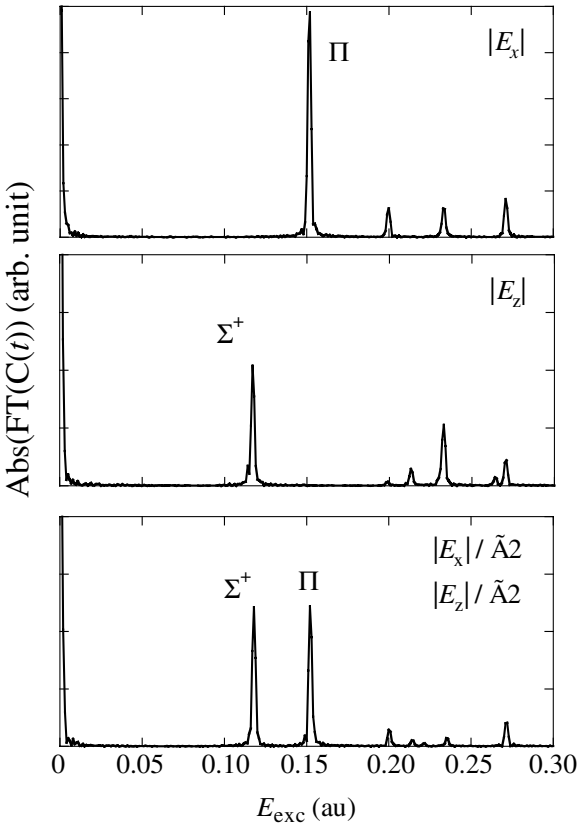

Figure 4. The effect of polarization of the pulse exhibited in the frequency domain. Shown is the excitation spectrum for three different polarizations. Top panel: polarization perpendicular to the bond, $|E_x| = 0.025$ au. Middle panel: polarization along the bond, $|E_z| = 0.025$ au. Bottom panel: polarization along the zx-direction, $|E_x| = 0.025/\sqrt{2}$ au and $|E_z| = 0.025/\sqrt{2}$au.

$\langle z\rangle(t) = \langle\Psi(t)|N^{-1}\sum_{i=1}^{N} z_i|\Psi(t)\rangle$. But the center of charge varies with time due to the beating between the ground, S_0, and first excited, S_1, Σ^+ states and this variation is used here as a diagnostic of the electron dynamics

$$\begin{aligned}\langle z\rangle(t) = \langle\Psi(t)|N^{-1}\sum_{i=1}^{N} z_i|\Psi(t)\rangle &= |c_0|^2\langle S_0|N^{-1}\sum_{i=1}^{N} z_i|S_0\rangle + |c_1|^2\langle S_1|N^{-1}\sum_{i=1}^{N} z_i|S_1\rangle \\ &+c_0^* c_1\langle S_0|N^{-1}\sum_{i=1}^{N} z_i|S_1\rangle\exp(-\mathrm{i}E_{\mathrm{exc}}t) + c_0 c_1^*\langle S_1|N^{-1}\sum_{i=1}^{N} z_i|S_0\rangle\exp(\mathrm{i}E_{\mathrm{exc}}t) + \cdots \\ &= |c_0|^2\langle S_0|N^{-1}\sum_{i=1}^{N} z_i|S_0\rangle + |c_1|^2\langle S_1|N^{-1}\sum_{i=1}^{N} z_i|S_1\rangle \\ &+2\left|c_0 c_1\langle S_0|N^{-1}\sum_{i=1}^{N} z_i|S_1\rangle\right|\cos(E_{\mathrm{exc}}t+\phi_{\mathrm{mol}}) + \cdots . \end{aligned} \tag{7}$$

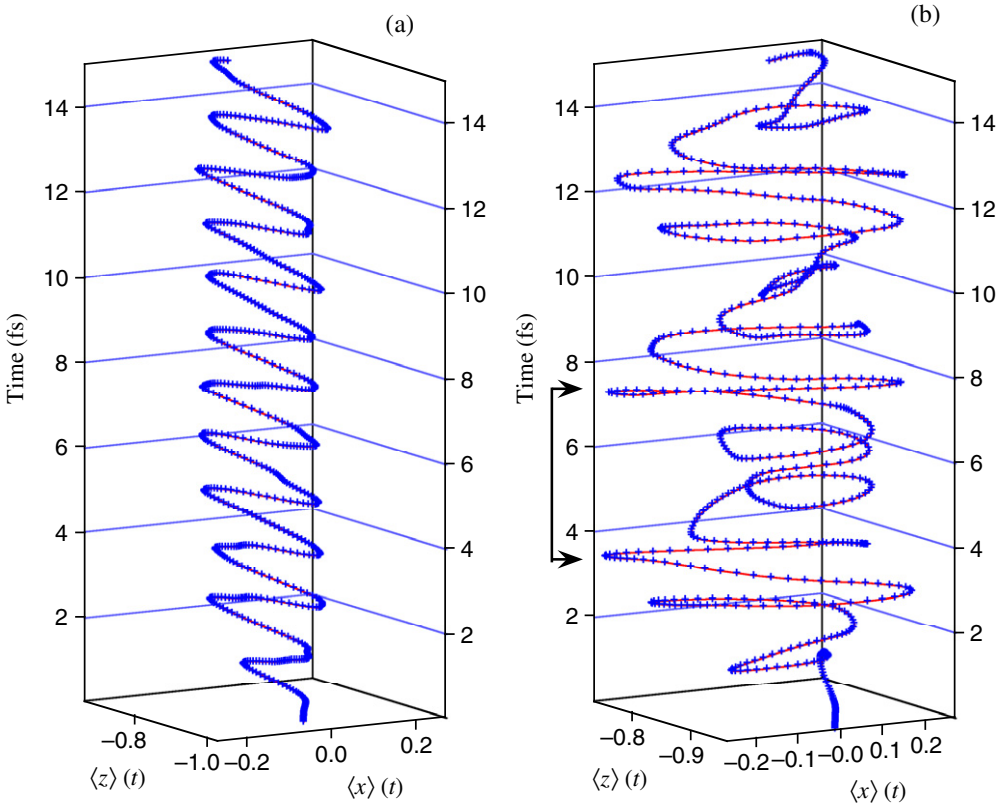

Figure 5. A three-dimensional plot of the motion of the electronic dipole of LiH. Shown are the x- and z-components of the dipole as time unfolds. The pump pulse is short, about 1 fs, with a phase shift of $\phi = -\pi/3$ and of intermediate intensity ($|E| = 0.025$ au). This pulse is used here because it puts a significant amplitude into the lowest excited Σ and even more into the Π state and yet it hardly excites any higher-lying states. (a) A pump pulse polarized in the z-direction. The dipole oscillates along z and there is no component along the x-axis. (b) A pump polarized along the xz-direction. The longest period is a rotation of the dipole about the axis of the molecule with a period of about 4 fs. Using the same intensity but a longer pulse and/or using a much more intense pulse produces a motion that is more multiply periodic because more excited states are significantly populated.

Here $E_{\rm exc}$ is the excitation frequency of the lowest Σ^+ state, 0.114 au as reported in table 1, and $\phi_{\rm mol}$ is the phase of the matrix element of the transition dipole, $\langle S_1|N^{-1}\sum_{i=1}^{N} z_i|S_0\rangle$, if there is one plus the phase of $c_0^* c_1$ [18]. The last plus sign indicates that other, higher-lying Σ excited states can contribute to the sum and that they will do so when the pulse intensity is high and multiphoton transition probabilities are not small. It is already implied by figures 1 and 4 and it is shown explicitly in figure 5 that it is possible to operate in a regime where there is one clear beat term in equation (7). Figure 5 is drawn for an intermediate intensity ($|E| = 0.025$ au) and a short, 40 au or about 1 fs in duration, pulse. It requires at least a doubling of the intensity or

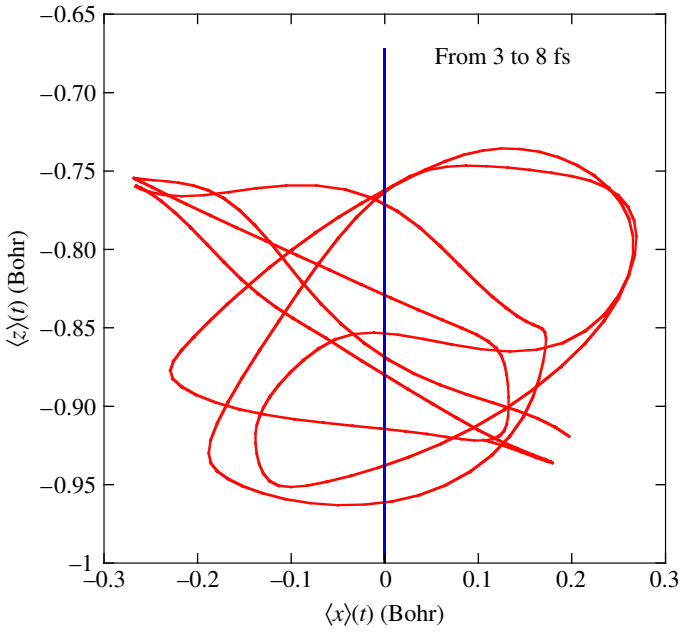

Figure 6. The electronic dipole of LiH plotted in the zx-plane at equally spaced time points. This is a projection of figure 5 on to the plane. It makes reading the periods harder but it highlights the contrast between the two laser polarizations. A pump polarized along z cannot create a dipole along the x-axis. Rather, the dipole oscillates with a short period along the z-axis. A pump polarized along zx creates a dipole that rotates with a longer period about the bond.

an increase in the duration of the pulse (to a level where the GS is extensively depleted) before higher excited states make the motion of $\langle z\rangle\ (t)$ multiply periodic.

The beat frequency implied by equation (7) is high because it is the excitation frequency of S_1, 0.114 au, as expected for an interference between an excited state and the GS. The essential point is therefore not the dynamics shown in figure 5(a) but the contrast between figures 5(a) and (b). The results shown in figure 5(b) are for a laser polarized in the xz-direction whereby a coherent superposition of the first excited Σ^+ and Π states is accessed. Due to the excitation of the Π state, charge is expected to move off the z-axis and in the x-direction as is clearly seen. The motion is multiply periodic but a high amplitude component with a long period of about 4 fs stands out. This is the beating between the first excited Σ^+ and Π states at a frequency of, cf table 1, $0.152 - 0.118 = 0.034$ au. The about fourfold faster periodic motion also seen in figure 5(b) is the beating with the GS.

The electronic motion set up when a coherent superposition of the first excited Σ^+ and Π states is pumped is essentially a rotation of the electronic density about the H atom. This is best examined in terms of the two components of the dipole. Along the z-axis, the dipole (= center of charge cloud) moves back and forth from about the location of the H atom towards the Li atom. Along the x-axis, the dipole moves up and down perpendicular to the bond (which is at $x = 0$).

The steering of the electronic dynamics that is made possible by the polarization is visualized in another manner in figure 6. This shows the same data as figure 5 but as a parametric

representation of the dipole in the z–x-plane. In such a projection, it is less easy to identify the periods of the motion. But this way of plotting makes it very clear that for a polarization along z the electronic dipole oscillates exclusively along the z-axis without any component along the x-axis. For a pump polarized in the zx-direction, there is clear rotational motion of the dipole about the H atom.

Using a different polarization, it is also possible to excite a wave packet that rotates about the bond without moving in the z-direction. This requires a pulse polarized in the xy-plane and such a pulse creates a coherent superposition of Π states. The results are shown in figure 7. The strength of the field $|E|$ is 0.025 au. Two aspects of control are shown. First suppose that we maintain the field shape as in equation (3). Then the center of charge $\langle \mathbf{r} \rangle(t) = \langle \Psi(t) | \sum_{i=1}^{N} \mathbf{r}_i | \Psi(t) \rangle / N$ will oscillate with equal phase along the x- and y-directions (see upper panel of figure 7). The same is true when a phase difference, $\Delta\phi$ of π is introduced between the x- and the y-components of the pump pulse. Suppose however, we use a field that is circularly polarized. Then one can set the charge rotating in the x–y-plane as shown in the bottom panel of figure 7 where the phase difference $\Delta\phi$ between the x- and the y-components of the pump pulse is $\pi/2$.

This section documented that coherent excitation of superpositions of Σ^+ and Π states of LiH is possible with high probability and yet at such laser intensities that the motion of the electronic wave packet remains amenable to analysis. In particular, it is possible to pump a high fraction of the GS to a coherent superposition of the two lowest Σ^+ and Π excited states. The interference of these two states results in an electronic wave packet that rotates about the H atom with a period of about 4 fs. In the next section, we discuss the probing of this motion and conclude that it is sufficient if one of the two pulses is shorter than the period of 4 fs. The other pulse, which in our simulations will be the probe, can be as long. Few-femtosecond pulses can therefore be used as a pump. An ultrafast pulse is only required as a probe.

4. Pump–probe spectroscopy

We use the control afforded by polarization and the selection rules that are still usefully valid as propensity rules up to quite high intensities, to probe a coherent superposition of the lowest excited Σ^+ and Π states. Time-resolved information is provided by the delay between the pump and probe pulses.

The pump pulse is polarized in the zx-direction with pulse parameters designed to have about equal amplitudes on the Σ^+ and Π states, as in figure 1(a). In the first series of computations a probe pulse polarized in the y-direction is applied. Figure 8 shows the location of the center of charge in the y-direction, $\langle y \rangle(t) = \langle \Psi(t) | N^{-1} \sum_{i=1}^{N} y_i | \Psi(t) \rangle$ when there is no probe and when a probe polarized in the y-direction whose envelope peaks at $\Delta t = 3.5$ fs after the pump peak. It is clear that the probe sets up an oscillating dipole in the y-direction where none was present before. (The probe is centered at the time $t_0 + \Delta t = 5.9$ fs but its envelope has a width so its effect is already felt earlier.) Analysis of the Fourier transform of the oscillating dipole shown in figure 8 verifies that the oscillations are due to interference of the $^1\Delta$ state with the lower-lying Σ^+ and Π states. To make sure that the pump can effectively access the Δ state the probe carrier is at a higher frequency, $\omega_p = 0.21$ au, so that the Δ state ($E_\Delta = 0.35$ au, see table 1) can be accessed by a $1+1$ photon process where the first photon is from the pump, $\omega_0 = 0.13$ au. Using a probe at a shorter wavelength has two further advantages. One is that one can interpret the results using one-photon selection rules. The second advantage is that

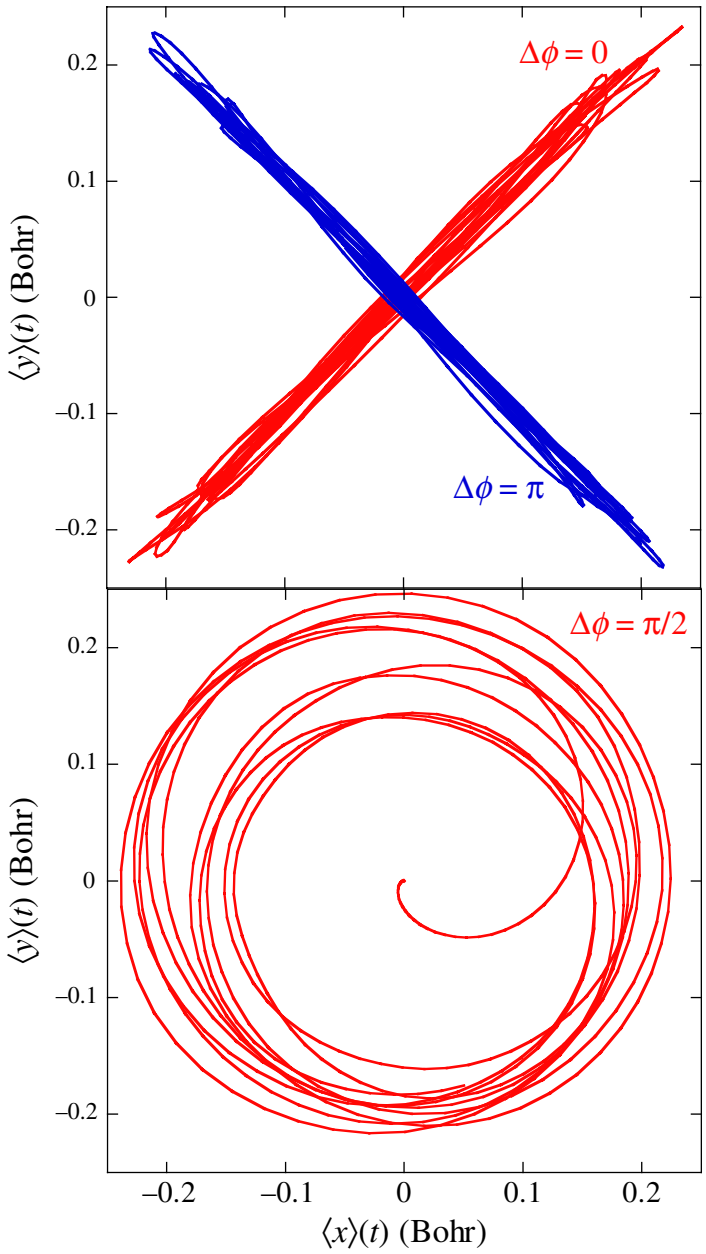

Figure 7. Same as figure 6 but for a pump pulse polarized in the xy-plane. This figure shows the control that can be exercised by polarization and by polarization and phase. The upper panel shows just the role of polarization and of a phase shift, $\Delta\phi = \pi$ between the x- and the y-components of the pulse. The center of charge oscillates along the bisector of the x–y-plane. The lower panel shows how the introduction of a phase shift of $\pi/2$ between the x- and y-components of the field sets the electronic wave packet rotating about the LiH bond. For all three traces, the time interval shown is 10 fs.

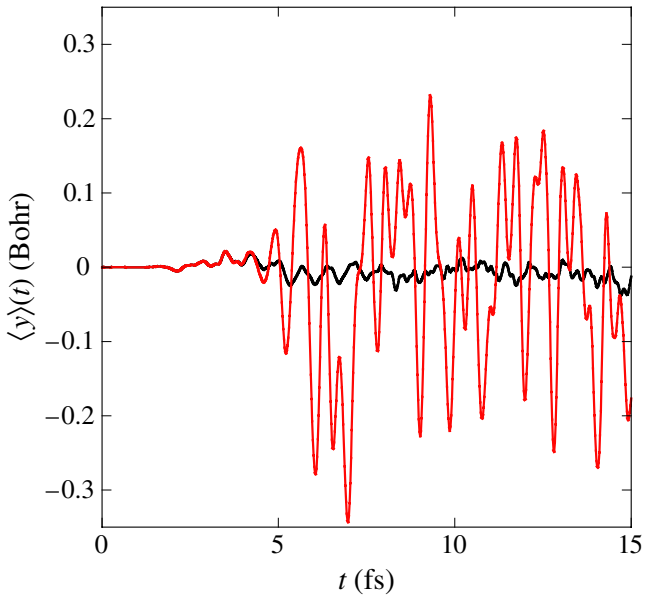

Figure 8. The dipole in the y-direction versus time in the presence and absence of a probe pulse polarized in the y-direction. The pump pulse is polarized in the xz-direction and therefore cannot give rise to a dipole in the y-direction. The very low amplitude oscillations in y that are present in the absence of the probe pulse are due to numerical noise in the integration procedure. The parameters of the pump are $|E_x| = |E_z| = 0.025/\sqrt{2}$ au and $t_0 = 100$ au, $\omega_0 = 0.13$ au. The probe pulse has the same intensity, $|E_y| = 0.025$ au, and a higher frequency $\omega_p = 0.21$ au and is centered at $t_0 + \Delta t = 245$ au so that it is delayed by 145 au (about 3.5 fs) from the peak of the pump pulse. Both the pump and the probe pulse have a width $\sigma = 0.68$ fs.

we propose to use a short probe pulse and this is easier to implement with a higher carrier frequency.

The first-order effect of a y-polarized probe pulse is to transfer population from the Π state to the $^1\Delta$ state, a transition with a relatively high transition dipole ($\langle ^1\Delta|\mu_y|^1\Pi\rangle = 1.656$ au). Another one-photon transition that is induced by the y-pulse is to access from the Σ^+ state to a second excited Π state and then to $^1\Delta$. This second state Π is about 0.25 au above the GS and the energy difference from it to $^1\Delta$ is about 0.1 au. A probe-induced transition from the first excited Σ^+ state to the $^1\Delta$ state is not first order allowed.

The pump pulse excites a coherent superposition of the lowest excited Σ^+ and Π states. The delay between the pump and probe is varied so that, since essentially not the pump but the probe can excite the $^1\Delta$ state, it serves as the readout for the amplitude of the Π state. The $^1\Delta$ state is autoionizing so that the excitation of this state is (relatively easily) monitored by the emitted photoelectrons.

To probe the coherent superposition of the lowest excited Σ^+ and Π states, we use a probe polarized along xy. The spectra as a function of the delay time Δt between the centers of the pump and probe pulses are shown in figure 9. The pump pulse is as in figures 1–3 with a field strength of $|\mathbf{E}| = 0.025$ au. The probe is short, $\sigma = 15/\sqrt{2}$ au, with a fourfold higher

power, $|\mathbf{E}| = 0.025$ au, and polarized in the xy-direction. The carrier frequency of the probe is 0.12 au and, because of the high intensity, this allows strong multiphoton transitions. The xy-polarization of the probe allows reaching the target $^1\Delta$ state from the excited Π states and from the GS and excited Σ^+ states with one-, two- and three-photon transitions. The time varying population of the $^1\Delta$ state as a function of the delay time between pump and probe is shown in the top panel of figure 9 because it is this variation that will need to be measured. The middle panel shows how the populations of the lowest excited Σ^+ and Π states respond to the presence of the probe pulse. These change because the probe bleaches these states by up-pumping to the $^1\Delta$ state. The probe is intense so it also affects the population of the GS, as shown in the lowest panel of figure 9. Not shown are changes induced by the pulse in the populations of the higher excited Σ^+ and Π states.

A simplistic analysis of why the probe is state-selective is to look only at selection rules. Below we do so and this is equivalent to using a 'white' probe without any frequency limitations. In the appendix, we carry out a model analysis of the enabling role of selection rules for a three-state model with the correct temporal envelope and carrier frequency of the probe pulse, but this analysis can only be done numerically. The results shown in figure 9 are therefore more realistic than those discussed in the appendix because all 210 determinants are kept in the computations leading to figure 9, while only three states are used in the appendix. The model used in the appendix is similar in spirit to what is known as the STIRAP excitation scheme [80, 81]. The one feature brought in by the model and not evident from selection rules alone is the important role of the carrier frequency of the probe pulse in determining the influence of the time delay between pump and probe on the observed spectrum.

We start the analysis of the role of selection rules with a simple approximation for the wavefunction at a delay Δt after the pump pulse:

$$\Psi(\Delta t) = C_\Sigma \exp(-\mathrm{i}E_\Sigma \Delta t)\,|\Sigma\rangle + C_\Pi \exp(-\mathrm{i}E_\Pi \Delta t)\,|\Pi\rangle + C_{\mathrm{GS}} \exp(-\mathrm{i}E_{\mathrm{GS}} \Delta t)\,|\mathrm{GS}\rangle\,. \tag{8}$$

This retains only the GS and the two (stationary) excited states of interest.

We then consider an intense probe pulse $\mathbf{E}$ short enough that it can be regarded as a source of (coherent) white light. We express the polarization of the probe as $\mathbf{E}_1 = ax + by$. The subscript 1 is for use below to designate the one photon selection rule. The two-photon term is $\mathbf{E}_2 = (ax + by)^2 = a^2x^2 + 2abxy + b^2y^2$. If only the y-component of the field takes from the first excited Π state to the target Δ state and if only xy takes from the first excited Σ to Δ, then the transition probability to the target Δ state is

$$\begin{aligned}|\langle\Delta\,|\mathbf{E}\,|\Psi\,\rangle|^2 &= |bC_\Pi\,\langle\Delta\,|y\,|\Pi\,\rangle|^2 + |2abC_\Sigma\,\langle\Delta\,|xy\,|\Sigma\,\rangle|^2 \\ &\quad + |4abb^*C_\Pi C_\Sigma\,\langle\Delta\,|y\,|\Pi\,\rangle\,\langle\Delta\,|xy\,|\Sigma\,\rangle|\cos(\Delta t(E_\Pi - E_\Sigma) + \varphi)\,.\end{aligned} \tag{9}$$

If the field is intense enough that three-photon transitions are not small, then there will be a third term describing transitions from the GS to the Δ state.

The yield of the Δ state, $|\langle\Delta\,|E\,|\Psi\,\rangle|^2$, monitors the beat term. If three-photon transitions are allowed, then there is a second beat term. In figure 9, which includes all states, there is a superposition of several beat terms and so the result is not as large a modulation as shown in equation (9).

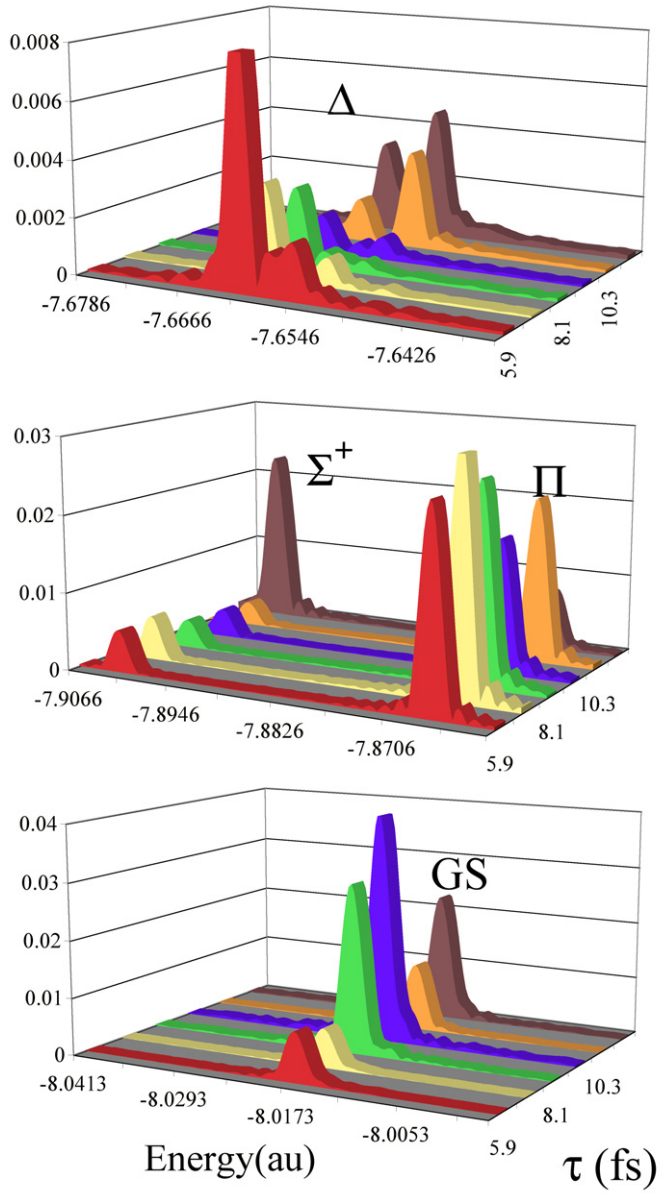

Figure 9. The role of the delay between the pump and probe. Top panel: the occupation of the ionizing state for different delay times. The pump pulse is the same as the one used in figure 8. The probe pulse is polarized in the xy-plane; its intensity is higher than in figure 8: $|E_x| = |E_z| = 0.05/\sqrt{2}$ au; and its width is shorter than in figure 8: $\sigma = 0.26$ fs. We regard the figure as a photoelectron spectrum and the oscillation in the population of the $^1\Delta$ state versus delay time as reflecting the coherent superposition of states set up by the pump pulse. Middle panel: the response of the populations of the lowest excited Σ^+ and Π states to the probe pulse. Bottom panel: for the GS. The panels show that the second pulse is not a weak probe but shifts populations in a significant way. By using a probe polarized in different directions, we can take advantage of the selection rules and so probe different aspects of the electron dynamics.

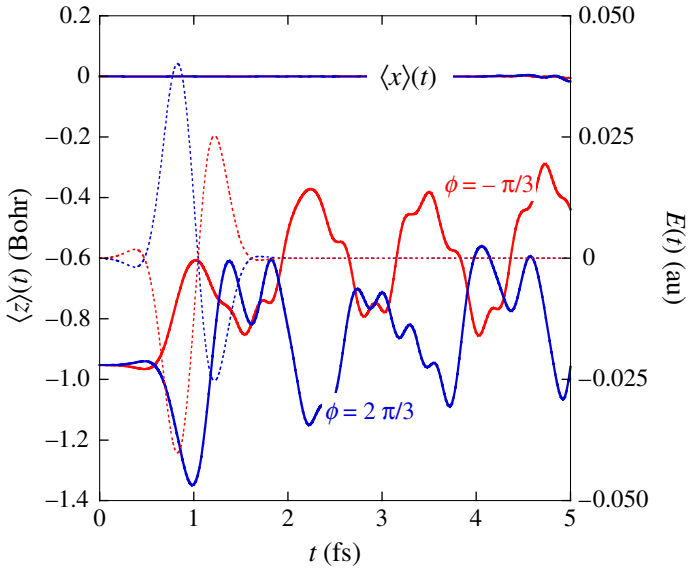

Figure 10. High amplitude steering of the charge density along the LiH bond by a strong pump pulse, $|\mathbf{E}| = 0.05$ au. Shown are the profiles of two fields along the z-direction versus time. The two fields are identical, barely more than one cycle pulses, but with different phases $\phi = -\pi/3$ and $\phi = 2\pi/3$, as defined in equation (3). The choice of phase means that the two fields oscillate in opposite directions along the z-axis as seen in the plot. The field pulls the charge density preferentially in the direction in which its amplitude is larger or smaller, depending on the sign of the transition dipole. Physically, this means that the two opposite fields send the charge density either towards the Li nucleus or away from it.

The dipole matrix elements are available from MOLPRO and the C coefficients in equation (8) can be varied by choice of the polarization and phase of the pump, as shown in figure 11 below. The ratio a/b is determined by the polarization and the frequency spectrum of the probe. Here, the spectrum is taken to be flat. In the appendix, we do a more realistic job.

5. Phase control

It is not yet possible to experimentally generate a nearly one-cycle pulse in the energy range of interest for electronic spectroscopy, but progress is being made [44, 45]. The problem is that it is not possible to squeeze several cycles of near-UV light into an envelope whose width in time is in the sub-femtosecond to few-femtosecond range. With just one cycle or so, the frequency spectrum of the pulse is rather broad and does not have a protruding maximum. For the present formalism, this spectrum is well defined and, in this section, it is shown that pulses for which $\omega_0\tau$ is not much over 2π allow us an even finer steering of the electronic density. This control is achieved by a judicious choice of the phase ϕ of the carrier wave, see equation (3).

To illustrate the control that may be possible, we contrast the results of computations at two values of the phase $\phi = -\pi/3$ and $\phi = 2\pi/3$. The temporal shape of the two pulses is shown in figure 10. The laser field oscillates about the z-direction. Initially the center of the charge

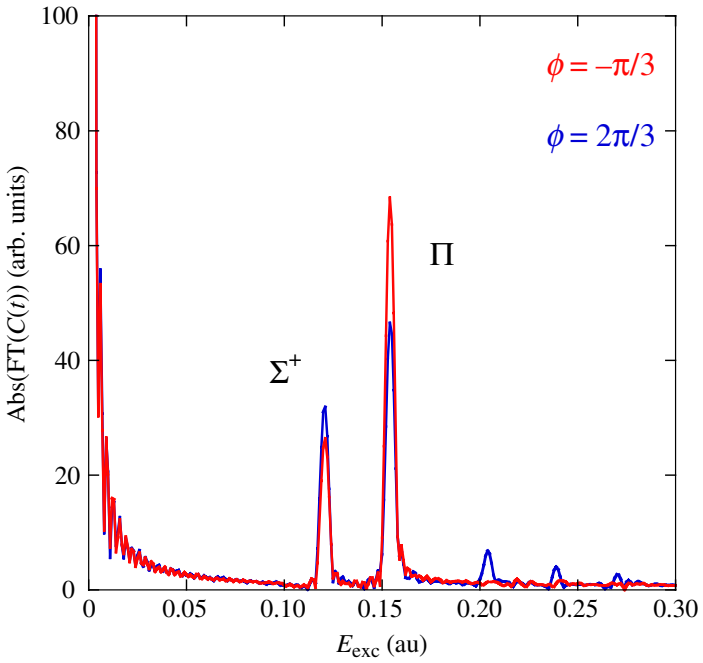

Figure 11. Phase control for a weaker pulse so that the control is even more selective. Examination of the spectrum shows that when the pulse is polarized in the xz-plane and for a moderate strength ($|E| = 0.025$ au), short ($t = 0.26$ fs) pulse, a phase shift of $-\pi/3$ gives a population ratio for Π/Σ+ of 2.7, while $2\pi/3$ gives a ratio of 1.4.

density is towards the H nucleus. Depending on the sign of the laser field at the time when its amplitude is maximal, it sends the electronic density even further away from the Li nucleus, which is roughly at $z = 0$, or, as in figure 3, the field sends the density towards the Li. As is to be expected for a field in the z-direction, $\langle x \rangle(t) = 0$ throughout.

Figure 11 shows a different manifestation of the phase control and it shows this for a weaker pulse so that the control is even more selective. Examination of the spectrum shows that when the pulse is polarized in the xz-plane and for a moderate strength ($|E| = 0.025$ au), short ($\tau = 0.26$ fs) pulse, a phase shift of $-\pi/3$ gives a population ratio for Π/Σ^+ of 2.7, while $2\pi/3$ gives a ratio of 1.4.

Finally, note that figure 7 also shows phase control, but in this case it is different phases for different field components. By varying the relative phase of the x- and y-components of the field, one can change the nature of the electronic dynamics from a linear to a circular motion.

6. Concluding remarks

Detailed computational results for the response of the four-electron LiH molecule to a few-cycle intense UV pulse are provided by a time-dependent multiconfiguration Hartree–Fock method using a large basis set that is, moreover, time-adaptive. The pulse intensity, duration, polarization and phase of carrier frequency can all be tuned to steer the motion of the electrons. A physical understanding of the effects of the pump is possible, because even at higher intensities, selection

rules provide useful guidance as to which states are accessed and to what extent. Furthermore, unless the pulse is ultraintense, the dynamics of the electronic wave packet has very few dominant characteristic frequencies so that its principal components of motion are readily visualized. For example, it is shown possible to direct the valence electrons to move along the Li–H bond or, by using a different pump polarization, normal to it. When the laser is polarized other than along the bond, the result is a rotation of the charge density. Shifting the phase of the carrier wave drives the electrons towards the Li nucleus or away from it. The resulting coherent dynamics induced by the pump pulse can be usefully probed by a delayed probe pulse. By means of probe pulse parameters such as polarization that are different from the pump pulse, detailed access to the more intimate aspects of the electron dynamics is possible.

Acknowledgments

MN thanks the DFG for funding under project SPP 1145. This collaborative work was carried out under the auspices of the German–Israeli James Franck program on Laser–Matter Interaction. Computational resources for this research were provided to FR and RDL by the MOLDYNLOGIC STREP FET-Open EC project (http://www.moldynlo.ulg.ac.be). FR thanks FNRS 1.5.187.05 for partial support.

Appendix. Three-level model of probe action

The full numerical results when incorporating the probe pulse are complicated by the contribution of high frequency beat terms due to transitions out of the GS. In the three-level model, we neglect these and allow only three states: the lowest excited $^1\Sigma^+$ and $^1\Pi$ states, labeled below as states 1 and 2, and the target $^1\Delta$ state, state 3. We use the energies and the transition dipole from the MOLPRO computation as given in table 1 and summarized here. For the energies $E_1 = -7.8887$ au, $E_2 = -7.8525$ au and $E_3 = -7.6469$ au, and for the transition dipole moments $\mu_{12} = -1.75$ au (polarized along x) and $\mu_{23} = +1.65$ au (polarized along y), there is no direct transition dipole from state 1 to 3.

We integrate the time-dependent Schrödinger equation for the three-level system

$$\mathrm{i}\frac{\mathrm{d}\mathbf{c}}{\mathrm{d}t} = \mathbf{H}\mathbf{c},$$

by going to the interaction picture. This allows us to identify clearly the two important frequencies in the problem, where E_c is the energy of a probe photon and we use $\hbar = 1$

$$\omega_{12} = (E_1 - E_2 + E_\mathrm{c}), \qquad \omega_{23} = (E_2 - E_3 + E_\mathrm{c}). \tag{A.1}$$

The amplitudes in this picture are $\tilde{c}_i = \exp(-\mathrm{i}E_i t)c_i$. Then

$$\mathrm{i}\frac{\mathrm{d}\tilde{\mathbf{c}}}{\mathrm{d}t} = \begin{pmatrix} 0 & \mu_{12}\,|E\,(t)|\exp\left(-\mathrm{i}\omega_{12}t\right) & 0 \\ \mu_{12}\,|E\,(t)|\exp\left(\mathrm{i}\omega_{12}t\right) & 0 & \mu_{23}\,|E\,(t)|\exp\left(-\mathrm{i}\omega_{23}t\right) \\ 0 & \mu_{23}\,|E\,(t)|\exp\left(\mathrm{i}\omega_{23}t\right) & 0 \end{pmatrix}\tilde{\mathbf{c}}, \tag{A.2}$$

where the probe field is

$$E\,(t) = |E\,(t)|\exp(-\mathrm{i}E_\mathrm{c}t) = |E|\exp\left(-\left(t - t_\mathrm{probe}\right)/\sigma^2\right)\exp(-\mathrm{i}E_\mathrm{c}t).$$

The center of the probe is delayed by Δt from the center of the pump $t_\mathrm{probe} = t_0 + \Delta t$.

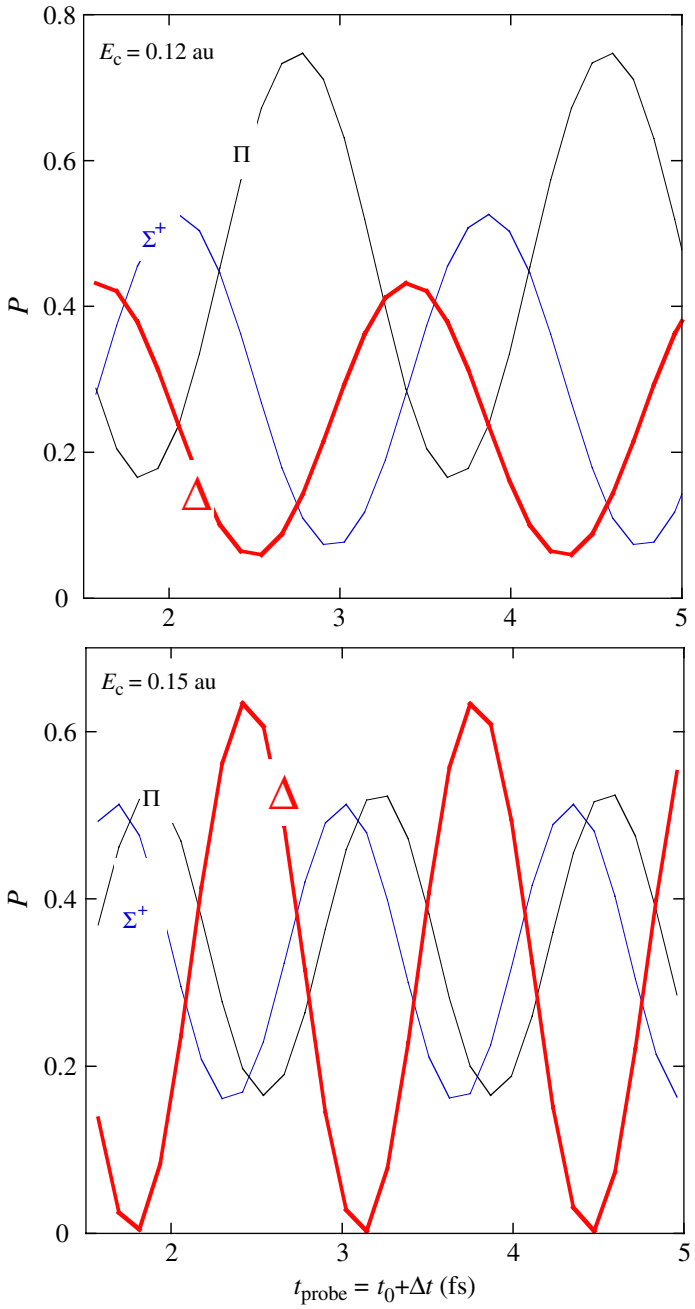

Figure A.1. Population of the three states Σ^+, Π and Δ as indicated, computed for a time long after the end of the probe pulse using equation (A.2), for different delay times, t_{probe}, between the pump and the probe pulses. The amplitudes of the Σ^+ and Π states created by the pump pulse are taken to be $1/\sqrt{2}$. Top panel: $E_c = 0.12$ au, which leads to a period of ≈ 2 fs (see equation (A.1)). Bottom panel: $E_c = 0.15$ au (the period is 1.33 fs).

Using the same data as for figure 9, we have $(E_2 - E_1 - E_c) = -0.0838$ au and $(E_3 - E_2 - E_c) = 0.0856$ au which is a period of 2 fs. The results are shown in figure A.1 (top panel). By changing the carrier frequency to $E_c = 0.15$ au, we can change the two frequencies to make them clearly different, $(E_2 - E_1 - E_c) = -0.1138$ au and $(E_3 - E_2 - E_c) = 0.0556$ au. The results are shown in figure A.1 (bottom panel).

The excited states of LiH and their excitation energy E_{exc} (with reference to the $^1\Sigma^+$ GS, at -8.00270 au) were computed using MOLPRO [76] at the multi (8, 3, 3, 2) level [82, 83], (the notation means that the 8σ, 3π and 2δ MOs are included in the orbital subspace and the core orbital of Li is not frozen) for four active electrons with a Cartesian 6–311++G(2df,2p) [67]–[70] basis at the internuclear distance of $R = 1.63$ Å. For more general references on the complete adaptive space self-consistent field (CASSCF) methods implemented in MOLPRO, see [83]–[85]. Including the GS, ten states are computed simultaneously at this level: six $^1\Sigma^+$, three $^1\Pi$ and one $^1\Delta$ states. The permanent dipole of the GS is 2.224 au and other permanent and transition dipoles are as shown, where the molecule is along the z-axis. In the MCTDHF computation, the basis set used is the same as in the MOLPRO computation. The results as shown are from figures 1(a) and (b). The energies computed using MOLPRO are seen to agree well with the energies obtained by Fourier transform of the autocorrelation of the wavefunction pumped by the more intense excitation pulse ($|E| = 0.05$ au) polarized at 45° in the xz-plane. The dependence on the pulse intensity is discussed in connection with figure 2.

References

[1] Stwalley W C and Zemke W T 1993 *J. Phys. Chem. Ref. Data* **22** 87–112
[2] Mulliken R S and Ermler W C 1997 *Diatomic Molecules Results of Ab Initio Computations* (New York: Academic)
[3] Boys S F and Handy N C 1969 *Proc. R. Soc. Lond.* A **311** 309
[4] Bender C F and Davidson E R 1968 *J. Chem. Phys.* **49** 4222–9
[5] Docken K K and Hinze J 1972 *J. Chem. Phys.* **57** 4928–36
[6] Meyer W and Rosmus P 1975 *J. Chem. Phys.* **63** 2356–75
[7] Yardley R N and Balint-Kurti G G 1976 *Mol. Phys.* **31** 921–41
[8] Stewart R F, Watson D K and Dalgarno A 1975 *J. Chem. Phys.* **63** 3222–7
[9] Gadea F X 2006 *Theor. Chem. Acc.* **116** 566–75
[10] Nest M, Padmanaban P and Saalfrank P 2007 *J. Chem. Phys.* **126** 214106
[11] Nest M, Klamroth T and Saalfrank P 2005 *J. Chem. Phys.* **122** 124102
[12] Mulliken R S 1936 *Phys. Rev.* **50** 1028
[13] Desouter-Lecomte M, Dehareng D, Leyh-Nihant B, Praet M T, Lorquet A J and Lorquet J C 1985 *J. Phys. Chem.* **89** 214–22
[14] Yarkony D R 1996 *Rev. Mod. Phys.* **68** 985–1013
[15] Haas Y, Klessinger M and Zilberg S (ed) 2000 *Conical Intersections in Photochemistry, Spectroscopy, and Chemical Dynamics* (Amsterdam: Elsevier)
[16] Worth G A and Cederbaum L 2004 *Annu. Rev. Phys. Chem.* **55** 127–58
[17] Domcke W, Yarkony D R and Koppel H (ed) 2004 *Conical Intersections: Electronic Structure, Dynamics and Spectroscopy* (Singapore: World Scientific)
[18] Levine R D 2005 *Molecular Reaction Dynamics* (Cambridge: Cambridge University Press)
[19] Remacle F and Levine R D 2006 *Proc. Natl Acad. Sci. USA* **103** 6793–8
[20] Yudin G L, Bandrauk A D and Corkum P B 2006 *Phys. Rev. Lett.* **96** 063002

[21] Hentschel M, Kienberger R, Spielmann C, Reider G A, Milosevic N, Brabec T, Corkum P, Heinzmann U, Drescher M and Krausz F 2001 *Nature* **414** 509–13
[22] Niikura H, Legare F, Hasbani R, Bandrauk A D, Ivanov M Y, Villeneuve D M and Corkum P B 2002 *Nature* **417** 917–22
[23] Baltuska A *et al* 2003 *Nature* **421** 611–5
[24] Niikura H, Legare F, Hasbani R, Ivanov M Y, Villeneuve D M and Corkum P B 2003 *Nature* **421** 826–9
[25] Kienberger R *et al* 2004 *Nature* **427** 817–21
[26] Sekikawa T, Kosuge A, Kanai T and Watanabe S 2004 *Nature* **432** 605–8
[27] Kling M F *et al* 2006 *Science* **312** 246–8
[28] Yudin G L, Chelkowski S, Itatani J, Bandrauk A D and Corkum P B 2005 *Phys. Rev.* A **72** 051401
[29] Kienberger R, Uiberacker M, Goulielmakis E, Baltuska A, Drescher M and Krausz F 2005 *J. Mod. Opt.* **52** 261–75
[30] Siedschlag C, Muller H G and Vrakking M J J 2005 *Laser Phys.* **15** 916–25
[31] Krausz F and Ivanov M 2008 *Rev. Mod. Phys.* to be published
[32] Niikura H, Villeneuve D M and Corkum P B 2006 *Phys. Rev.* A **73** 021402
[33] Dudovich N, Smirnova O, Levesque J, Mairesse Y, Ivanov M Y, Villeneuve D M and Corkum P B 2006 *Nat. Phys.* **2** 781–6
[34] Baker S, Robinson J S, Haworth C A, Teng H, Smith R A, Chirila C C, Lein M, Tisch J W G and Marangos J P 2006 *Science* **312** 424–7
[35] Sansone G *et al* 2006 *Science* **314** 443–6
[36] Scrinzi A, Ivanov M Y, Kienberger R and Villeneuve D M 2006 *J. Phys. B: At. Mol. Opt. Phys.* **39** R1–37
[37] Bucksbaum P H 2007 *Science* **317** 766–9
[38] Goulielmakis E, Yakovlev V S, Cavalieri A L, Uiberacker M, Pervak V, Apolonski A, Kienberger R, Kleineberg U and Krausz F 2007 *Science* **317** 769–75
[39] Yudin G L, Bandrauk A D and Corkum P B 2006 *Phys. Rev. Lett.* **96** 063002
[40] Itatani J, Levesque J, Zeidler D, Niikura H, Pepin H, Kieffer J C, Corkum P B and Villeneuve D M 2004 *Nature* **432** 867–71
[41] Aseyev S A, Ni Y, Frasinski L J, Muller H G and Vrakking M J J 2003 *Phys. Rev. Lett.* **91** 223902
[42] Drescher M, Hentschel M, Kienberger R, Uiberacker M, Westerwalbesloh T, Kleineberg U, Heinzmann U and Krausz F 2004 *J. Electron Spectrosc. Relat. Phenom.* **137–40** 259–64
[43] Drescher M *et al* 2002 *Nature* **419** 803
[44] Remacle F, Kienberger R, Krausz F and Levine R D 2007 *Chem. Phys.* **338** 342–7
[45] Cavalieri A L *et al* 2007 *New J. Phys.* **9** 242
[46] Bandrauk A D, Chelkowski S and Nguyen H S 2004 *Int. J. Quantum Chem.* **100** 834–44
[47] Kling M F *et al* 2006 *Science* **312** 246
[48] Weitzel K M 2007 *ChemPhysChem* **8** 213–5
[49] Krause P, Klamroth T and Saalfrank P 2005 *J. Chem. Phys.* **123** 074105
[50] Barth I and Manz J 2006 *Angew. Chem. Int. Edn Engl.* **45** 2962–5
[51] Barth I, Manz J, Shigeta Y and Yagi K 2006 *J. Am. Chem. Soc.* **128** 7043–9
[52] Kuleff A I, Breidbach J and Cederbaum L S 2005 *J. Chem. Phys.* **123** 044111
[53] Hennig H, Breidbach J and Cederbaum L S 2005 *J. Chem. Phys.* **122** 249901
[54] Breidbach J and Cederbaum L S 2005 *Phys. Rev. Lett.* **94** 033901
[55] Kanno M, Kono H and Fujimura Y 2006 *Angew. Chem. Int. Edn Engl.* **45** 7995–8
[56] Sahnoun R, Nakai K, Sato Y, Kono H, Fujimura Y and Tanaka M 2006 *J. Chem. Phys.* **125** 184306
[57] Nakai K, Sahnoun R, Kato T, Kono H and Fujimura Y 2005 *J. Phys. Chem.* B **109** 13921–7
[58] Li X S, Smith S M, Markevitch A N, Romanov D A, Levis R J and Schlegel H B 2005 *Phys. Chem. Chem. Phys.* **7** 233–9
[59] Yamaki M, Hoki K, Ohtsuki Y, Kono H and Fujimura Y 2005 *J. Am. Chem. Soc.* **127** 7300–1
[60] Kato T and Kono H 2004 *Chem. Phys. Lett.* **392** 533–40

[61] Harumiya K, Kono H, Fujimura Y, Kawata I and Bandrauk A D 2002 *Phys. Rev.* A **66** 043403
[62] Kono H, Koseki S, Shiota M and Fujimura Y 2001 *J. Phys. Chem.* A **105** 5627–36
[63] Kono H, Sato Y, Tanak N, Kato T, Nakai K, Koseki S and Fujimura Y 2004 *Chem. Phys.* **304** 203–26
[64] Mercouris T, Komninos Y and Nicolaides C A 2007 *Phys. Rev.* A **75** 013407
[65] Mercouris T, Komninos Y and Nicolaides C A 2004 *Phys. Rev.* A **69** 032502
[66] Nicolaides C A, Mercouris T and Komninos Y 2002 *J. Phys. B: At. Mol. Opt. Phys.* **35** L271–9
[67] Frisch M J, Pople J A and Binkley J S 1984 *J. Chem. Phys.* **80** 3265–9
[68] Clark T, Chandrasekhar J, Spitznagel G W and Schleyer P V 1983 *J. Comput. Chem.* **4** 294–301
[69] Hay P J 1977 *J. Chem. Phys.* **66** 4377–84
[70] Wachters A J 1970 *J. Chem. Phys.* **52** 1033
[71] Seideman T and Hamilton E 2005 Relativistic nonlinear optics *Advances in Atomic Molecular and Optical Physics* vol 52 (Amsterdam: Elsevier) pp 289–329
[72] Kramer P and Saraceno M (ed) 1981 *Geometry of the Time-Dependent Variational Principle in Quantum Mechanics* (Berlin: Springer)
[73] Meyer H D and Worth G A 2003 *Theor. Chem. Acc.* **109** 251–67
[74] Beck M H, Jackle A, Worth G A and Meyer H D 2000 *Phys. Rep.* **324** 1–105
[75] Meyer H D, Manthe U and Cederbaum L S 1990 *Chem. Phys. Lett.* **165** 73–8
[76] Werner H-J and Knowles P J 2002 *MOLPRO Suite of Programs* version 2002.6
[77] Huber K P and Herzberg G 1979 *Molecular Spectra and Molecular Structure* (New York: Van Nostrand-Reinhold)
[78] Heller E J 1981 *Acc. Chem. Res.* **14** 368–75
[79] Levine R D and Kinsey J L 1991 *Proc. Natl Acad. Sci. USA* **88** 11133
[80] Remacle F and Levine R D 2006 *Phys. Rev.* A **73** 033820–7
[81] Vitanov N V, Halfmann T, Shore B W and Bergmann K 2001 *Annu. Rev. Phys. Chem.* **52** 763–809
[82] Werner H J and Knowles P J 1985 *J. Chem. Phys.* **82** 5053–63
[83] Knowles P J and Werner H J 1985 *Chem. Phys. Lett.* **115** 259–67
[84] Werner H J and Meyer W 1980 *J. Chem. Phys.* **73** 2342–56
[85] Werner H-J 1987 *Adv. Chem. Phys.* **69** 1